



Effect of Ceria on redox-catalytic property in mild condition: A solvent-free route for imine synthesis at low temperature

Hepeng Zhang^{a,b,*}, Chen Wu^{b,1}, Wenbin Wang^b, Jun Bu^b, Fengtao Zhou^b, Baoliang Zhang^{b,*}, Qiuyu Zhang^b

^a Research & Development Institute of Northwestern Polytechnical University in Shenzhen, Shenzhen 518057, PR China

^b School of Applied and Natural Sciences, Northwestern Polytechnical University, Xi'an 710129, PR China



ARTICLE INFO

Keywords:

Ceria
Imine synthesis
Mild conditions
Solvent-free
Redox catalysis

ABSTRACT

Five different nanocerias were prepared and used to catalyze the direct coupling of alcohol and amine to the corresponding imines under air atmosphere at low temperature. The catalytic efficiencies have great differences, CeO_2 prepared by coprecipitation at room temperature (called $\text{CeO}_2\text{-5}$) has the best catalytic activity, whose yield reaches 99% at 303 K for 36 h, 100 times higher than the nano-octahedras ceria (called $\text{CeO}_2\text{-4}$) and also higher than the catalytic performance of most reported catalysts. Such phenomena are ascribed to the higher acidic sites, specific surface area, and proportions of surface oxygen. The results of DRIFTS demonstrated that the alcohol oxidized to benzaldehyde was the rate determining step in this reaction. Furthermore, $\text{CeO}_2\text{-5}$ still shows excellent catalytic performance on 10-fold magnification experiments without any addition of solvent. Besides, it has the advantages of simple process, low energy consumption and practical scaling-up as well as good universality towards this kind of reaction, showing every prospect in industrial application.

1. Introduction

The past decades have witnessed a monumental achievement in the synthesis, morphology and catalytic abilities of ceria-based materials [1–6]. Over the preceding years, nanostructured CeO_2 with different morphologies, applicable in solid oxides fuel cells, oxygen storage materials, electrochemical devices and three-way catalysts [7–16], have intrigued increasingly tremendous interests from researchers worldwide. Intensive studies have shown that the widespread applications of ceria are linked to its relative abundance, exceptional acid-base and surface properties with the dynamically reversible $\text{Ce}^{3+}/\text{Ce}^{4+}$ redox pair. These properties also endow ceria with remarkable catalytic performance for various organic transitions, such as aldolization, the dehydration of alcohols and the alkylation of aromatic compounds. Nowadays there are considerable reports about the catalytic application of ceria in various kinds of reactions [17–26], most of which, however, demand high temperature and gas phase catalysis. The research on ceria used as catalysis in liquid organic reactions under mild conditions was very rare, especially the influence of different crystal plane and morphologies.

Imines and their derivatives, as key intermediates of N based reaction, have been widely applied to the reaction of reduction, addition,

condensation as well as in biological, agricultural and pharmaceutical fields [27–29]. Imine can be obtained not only by the direct reaction of carbonyl compounds and amines, but also through the aerobic oxidative coupling reaction of alcohols and amines [30,31]. The latter process is preferential and environmentally-benign as benzyl alcohol is cheaper and commercially available and water is the only by-product. But this reaction usually requires harsh reaction conditions, such as precious metal catalysis and pure oxygen for the low reactivity of benzyl alcohol. Tamura et al. [32] studied imine formation from benzyl alcohol and aniline at 303 K and 333 K under air using various metal oxides as catalysts and found that ceria delivers highest catalytic activity. The results showed that when the amount of ceria is 46% (W/W) of benzyl alcohol, the yield of the reaction is 75% at 303 K for 48 h, and 96% at 333 K for 24 h, respectively.

However, from economic and green chemistry points of view, several issues must be settled for the perfect deployment of ceria in the imines synthesis, including: (1) finding low-energy consuming, environmental-friendly and easy scaling-up preparation of ceria; (2) improving the catalytic activity of CeO_2 in mild conditions to reduce reaction time; (3) studying the magnification synthesis of imines from alcohols and amines under green ways (such as solvent free conditions); (4) enlarging the universality of ceria toward the imines synthesis; (5)

* Corresponding authors at: School of Applied and Natural Sciences, Northwestern Polytechnical University, Xi'an, 710129, PR China.

E-mail addresses: zhanghepeng@nwpu.edu.cn (H. Zhang), blzhang@nwpu.edu.cn (B. Zhang).

¹ These authors contributed equally to this work.

discovering the reaction mechanism toward the coupling reaction between benzyl alcohol and aniline.

Herein, for proposing some solutions to the problems discussed above, we prepared five kinds of ceria through hydrothermal method and modified precipitation [33] and compared their catalyzing efficiency using the coupling reaction of benzyl alcohol and aniline as a model. Results show that the ceria (CeO₂-5) prepared by precipitation at room temperature, which is energy saving and feasible of scaling-up, has the highest specific surface area (162 m²·g⁻¹) and the best catalytic capacity, with the yield of 89% for 24 h and 99% for 36 h at 303 K. Meanwhile, this CeO₂-5 has exhibited a good capability to magnification experiments without the addition of solvent. The relation between the properties and catalytic efficiency of these ceria and the catalytic mechanism were also discussed in this paper.

2. Experimental

2.1. Chemical reagents

Cerium (III) nitrate hexahydrate, Cerium (III) chloride heptahydrate and sodium phosphate tribasic dodecahydrate were purchased from Shanghai Shangpu Chemical Co., Ltd. Potassium hydroxide and sodium hydroxide were bought from Tianjin Fuchen Chemical Reagent Factory. Benzyl alcohol, aniline and mesitylene were all purchased from Sigma Company. The above reagents were of analytical grade and used directly without any further purification before the experiment. Deionized water used in the experiments was from local sources.

2.2. Experimental process

2.2.1. Preparation of CeO₂ nanocubes

The typical process for the preparation of cube nano-CeO₂ is as follows: 3.5 mmol Ce(NO₃)₃·6H₂O and 1.05 mol KOH were dissolved in 70 mL deionized water and stirred for 30 min with a magnetic stirrer. The obtained suspension was then transferred into a 100 mL Teflon-line stainless steel autoclave, which was sealed and maintained at 503 K for 24 h and then cooled to room temperature naturally. The resulting yellow precipitates were separated by centrifuging and washing with distilled water for three times. Finally, the products named as CeO₂-1 were dried by vacuum drying for 12 h and collected for further characterization.

2.2.2. Preparation of CeO₂ nanorods

2.2.2.1. Cerium nitrate as cerium source. The typical process for the preparation of CeO₂ nanorods is as follows: 3.5 mmol Ce(NO₃)₃·6H₂O and 1.05 mol KOH were dissolved in 70 mL deionized water and stirred for 30 min with a magnetic stirrer. The obtained suspension was then transferred into a 100 mL Teflon-line stainless steel autoclave, which was sealed and maintained at 413 K for 24 h and then cooled to room temperature naturally. The resulting yellow precipitates were separated by centrifuging and washing with distilled water for three times. Finally, the products named as CeO₂-2 were dried by vacuum drying for 12 h and collected for further characterization.

2.2.2.2. Cerium chloride as cerium source. The typical process for the preparation of CeO₂ nanorods is as follows: 3.5 mmol CeCl₃·7H₂O and 1.05 mol KOH were dissolved in 70 mL deionized water and stirred for 30 min with a magnetic stirrer. The obtained suspension was then transferred into a 100 mL Teflon-line stainless steel autoclave, which was sealed and maintained at 503 K for 24 h and then cooled to room

temperature naturally. The resulting yellow precipitates were separated by centrifuging and washing with distilled water for three times. Finally, the products named as CeO₂-3 were dried by vacuum drying for 12 h and collected for further characterization.

2.2.3. Preparation of CeO₂ nano-octahedras

The typical process for the preparation of CeO₂ nano-octahedras is as follows: 3.5 mmol Ce(NO₃)₃·6H₂O and 0.35 mmol Na₃PO₄·12H₂O were dissolved in 70 mL deionized water and stirred for 30 min with a magnetic stirrer. The obtained suspension was then transferred into a 100 mL Teflon-line stainless steel autoclave, which was sealed and maintained at 453 K for 10 h and then cooled to room temperature naturally. The resulting yellow precipitates were separated by centrifuging and washing with distilled water for three times. Finally, the products named as CeO₂-4 were dried by vacuum drying for 12 h and collected for further characterization.

2.2.4. Preparation of CeO₂ at room temperature

The typical process for the preparation of CeO₂ at room temperature is as follows: 16 mmol Ce(NO₃)₃·6H₂O dissolved in 5 mL deionized water and 14 mol KOH dissolved in 35 mL deionized water were mixed in a beaker without stirring. The suspension was then left at room temperature (293 K) for 48 h. The products named as CeO₂-5 were washed three times with distilled water and dried at 353 K for 24 h.

2.3. Catalytic reaction

According to the reference [32], the general synthesis process of imines is as follows: CeO₂ (50 mg) was added to the mixture of 1.0 mmol benzyl alcohol and 2.0 mmol aniline in 1.6 mL mesitylene in a reaction vessel under air. The obtained mixture was vigorously stirred at 303 K or 333 K. The reaction equation is shown in **Scheme 1**:

After reaction, the mixture was diluted with ethanol and centrifuged. The yield of the product and the conversion of the monomer were measured by high performance liquid chromatography.

2.4. Characterization

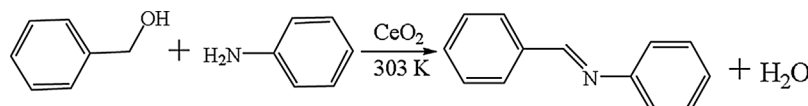
X-ray diffraction patterns (XRD) was recorded using X-ray powder diffraction (XRD-7000S from Shimadzu) to characterize the structure and crystallinity of the samples.

The transmission electron microscopy (TEM) and high resolution transmission electron microscopy (HRTEM) images were performed on Tecnai G2 F20 high resolution transmission electron microscopy to measure the morphology, size and the lattice spacing of the five CeO₂.

N₂-adsorption desorption isotherms and pore size distributions were obtained using the TriStar II 3020 specific surface area and pore size analyzer manufactured by Micromeritics, USA. The samples were degassed at 363 K for 24 h under vacuum before testing. The specific surface area and pore volume were calculated from the BET model, and the pore size distribution was calculated by density functional theory (DFT).

Hydrogen temperature-programmed-reduction (H₂-TPR), oxygen temperature-programmed-desorption (O₂-TPD) and pyridine temperature-programmed-desorption (pyridine-TPD) experiments were accomplished on the Auto Chem II 2920 chemical adsorber produced by Micromeritics, USA with a TCD (thermal conductivity detector).

In a typical H₂-TPR process, 50 mg sample powders were outgassed at 373 K for 30 min under an Argon flow (25 mL/min) and subsequently cooled down to 303 K. Then the temperature was raised to 1173 K with



Scheme 1. Synthesis of benzalaniline by benzyl alcohol and aniline.

a heating rate of 10 K/min under a hydrogen flow (10% in Argon, 50 mL/min) and the consumption of H₂ was recorded. The amount of H₂ consumption was quantified by calibrating the peak area against that of pure CeO₂ samples.

In a typical O₂-TPD experiment, 100 mg sample powders were preheated at 393 K for 1 h under an Argon flow (30 mL/min), followed by cooling down to 323 K in the same Argon flow and purging with an O₂ flow (10% in Argon, 50 mL/min) for 2 h and then changing to Argon flow (50 mL/min) until the baseline was stable. Then, the temperature was raised to 1173 K with a heating rate of 10 K/min under the same Argon flow.

In a typical pyridine-TPD experiment, 20 mg sample powders were preheated at 373 K for 30 min under a He flow (25 mL/min) and then cooled down to 373 K. Pyridine gas was produced by a vapor generator and introduced by a pulse injection with the He flow until saturation which was indicated by the stabilization of the TCD signal. The sample was subsequently held at 383 K for 1 h to eliminate the physically adsorbed pyridine. Then the temperature was raised to 1073 K with a heating rate of 10 K/min under the same He flow and the desorption of pyridine was detected.

In-situ IR spectra were collected on a Bruker Optics VERTEX 70 equipped with a liquid nitrogen-cooled MCT detector, using an in situ IR cell with CaF₂ windows, which was connected to a conventional gas flow system. The CeO₂ powder (~50 mg) were put into the DRIFTS cell under a N₂ flow (20 mL/min) and pretreated at 473 K for 30 min and then cooled down to 303 K before adsorption of probe molecules. All the IR spectra, referenced to a background spectrum of the CeO₂ samples, were collected every one minute.

Adsorption of pyridine: 200 μ L pyridine were injected into a vaporizer of 393 K and the pyridine vapor was brought into the in situ cell to the CeO₂ samples by a N₂ flow (20 mL/min) at 303 K and then the IR measurement was carried out.

Measurement of redox capacity: 5 μ L benzyl alcohol were injected into the samples under a N₂ flow (20 mL/min) at 333 K and the IR measurement began. Once the spectrum was stable, air was introduced into the IR cell, and the spectrum change was monitored until static spectra were observed. Then 10 μ L aniline were immitted into the sample and the difference among the spectra were scrutinized.

X-ray photoelectron spectroscopy (XPS) measurements were performed with an Axis Ultra DLD X-ray photoelectron spectroscopy manufactured by Kratos Company in the United Kingdom. The instrument used an Al K α ray light source to measure the total ambient gas pressure ($< 10^{-8}$ Pa).

¹H NMR spectra were recorded on Avian 400 MHz superconduction digital nuclear magnetic resonance instrument of Bruker, Germany. Deuterated chloroform (CDCl₃) was used as solvent and TMS was used as internal standard.

3. Results and discussion

3.1. Catalysts characterization

XRD patterns of the obtained five kinds of ceria are presented in Fig. 1. All diffraction peaks in Fig. 1 can be indexed to the face-centered cubic-phase CeO₂ (fluorite structure, JCPDS card no. 34-0394). The large and narrow diffraction peaks of CeO₂-1, CeO₂-2, CeO₂-3 and CeO₂-4 indicate good crystallinity while CeO₂-5 without any high-temperature treatment shows poor crystallinity.

To further confirm the morphology and crystallinity of these ceria, TEM and HRTEM (Fig. 2) analysis were employed. It can be observed in the Fig. 2-1a and Fig. 2-1b that CeO₂-1 has a uniform cube structure with average diameter of about 50 nm and the interplanar spacing of 0.2750 nm, which is in good accordance with the lattice parameter of the (200) facet. Besides, CeO₂-2 (Fig. 2-2a) has a rod-like structure with average length of about 400 nm. As presented in the HRTEM image in Fig. 2-2b, the obtained CeO₂-2 nanorods formed by agglomeration of

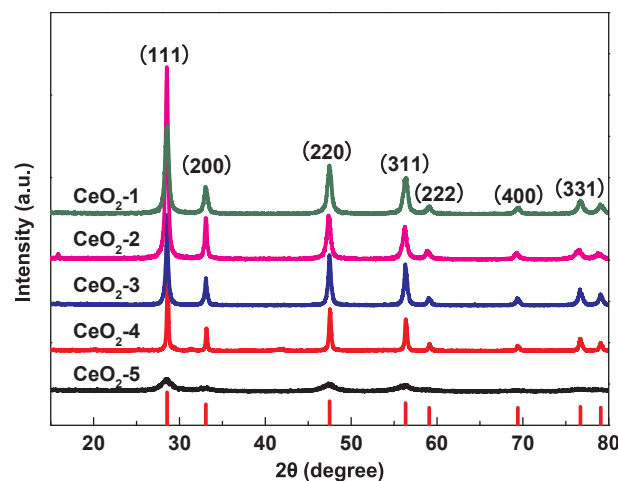


Fig. 1. XRD patterns of the five kinds ceria.

multiple nano-CeO₂ monocrystals. Moreover, CeO₂-3, which also shows a rod-like structure in its TEM image (Fig. 2-3a), has a diameter of about 60 nm and a length of about 5–7 μ m. It is clear in the HRTEM image (Fig. 2-3b) that CeO₂-3 also formed by agglomeration of multiple nano-CeO₂ monocrystals. Meanwhile, CeO₂-4 (Fig. 2-4a) has a pure octahedral morphology with the average particle size of about 200 nm. It is presented in the HRTEM image (Fig. 2-4b) that the lattice fringe parallel to the surface of CeO₂-4 displays interplanar distance of 0.3125 nm, which matches well with that of CeO₂ (111) plane. In addition, CeO₂-5 (Fig. 2-5a and 5b) is very small crystals with irregular single crystal shape.

H₂-TPR spectra of the CeO₂ in five different morphologies are compared in Fig. 3. It is clear that all these ceria have two adsorption peaks in the whole temperature range. The peak at low temperature is related to the chemisorbed oxygen species (the oxygen on the exposed crystal surface), and the peak at relatively higher temperature corresponds to the lattice oxygen species (the oxygen in the lattice of CeO₂ phase). The resulting O₂-TPD spectrum also showed that there were chemisorbed oxygen species on the surface of ceria (S1). It has been suggested that the chemisorbed oxygen species are more active than the lattice oxygen species, due to its higher mobility than the lattice oxygen [34]. From the H₂-TPR spectra, although each CeO₂ has two adsorption peaks for H₂, the temperature of the peak at low temperature zone appears to be different. CeO₂-5 shows the lowest first adsorption temperature (417 °C), followed by CeO₂-2 (435 °C) prepared by cerium nitrate and CeO₂-3 (451 °C) prepared by cerium chloride; the first adsorption temperature of cubic CeO₂-1 is 497 °C and the highest first adsorption temperature is octahedral CeO₂-4 (526 °C). The first adsorption temperature represents the temperature at which the surface oxygen reacts with H₂, where lower temperature is assigned to better oxidation ability of the material. Therefore, from the H₂-TPR results, it is clear that the oxidation abilities of the obtained CeO₂ in different morphologies decrease in the following order: CeO₂-5 > CeO₂-2 > CeO₂-3 > CeO₂-1 > CeO₂-4.

The surface acidity sites of these catalysts were measured by pyridine-TPD, and the capacity of pyridine adsorption in CeO₂-5 is 24.0 mmol·g⁻¹, higher than the other CeO₂ catalysts. FTIR spectra of adsorption pyridine are also compared (S2) to determine the type of the surface acidity sites. For CeO₂-5, the chemisorption pyridine with Brønsted acidic sites at 1540 cm⁻¹ is stronger than Lewis acidic sites at 1440 ~ cm⁻¹ – exactly the opposite of what is for CeO₂-1, CeO₂-2, CeO₂-3 and CeO₂-4 [35,36]. The intensity of the peaks of Brønsted acidic sites decreases in the following order: CeO₂-5 > CeO₂-2 > CeO₂-3 > CeO₂-1 ≈ CeO₂-4.

XPS analysis was performed in order to explore the difference on the catalytic capacities of ceria. Peaks corresponding to Ce 3d and O 1s are

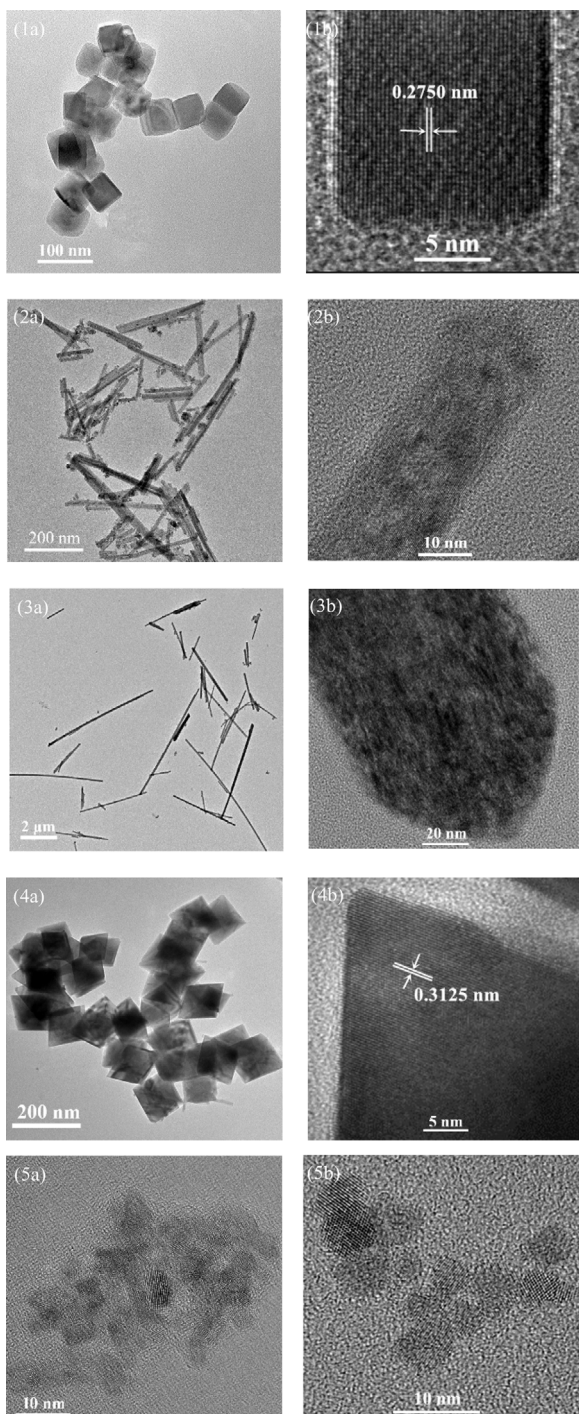


Fig. 2. TEM images (a), HRTEM images (b) of ceria: (1) CeO₂-1; (2) CeO₂-2; (3) CeO₂-3; (4) CeO₂-4; (5) CeO₂-5.

clearly displayed in S3, S4 and S5. In the Ce 3d spectra, (U, V), (U₂, V₂) and (U₃, V₃) are related to Ce⁴⁺ oxidation states [37], which belong to Ce 3d⁹4f² O 2p⁴, Ce 3d⁹4f¹ O 2p⁵ and Ce 3d⁹4f⁰ O 2p⁶, respectively. (U₁, V₁) and (U₀, V₀) are Ce³⁺ oxidation states, pertaining to Ce 3d⁹4f¹ O 2p⁵ and Ce 3d⁹4f¹ O 2p⁶, respectively [38]. The ion concentration of Ce³⁺ can be calculated by formula (1) according to the peak area corresponding to each fitting peak in the spectra [39]:

$$\frac{[\text{Ce}^{3+}]}{[\text{Ce}^{3+} + \text{Ce}^{4+}]} = \frac{(V_0, V_1, U_0, U_1) \text{peak area}}{\text{Total peak area}} \quad (1)$$

The O 1s XPS spectra are fitted into two kinds of peaks assigned to

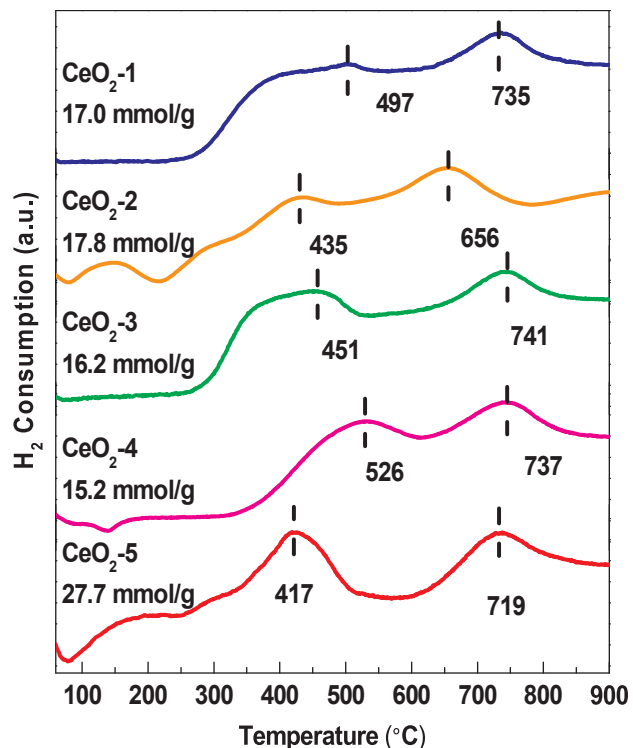


Fig. 3. H₂-TPR spectra of CeO₂ in different morphologies.

the lattice oxygen species at low binding energy (528.6–530.1 eV) and the chemisorbed oxygen species at high binding energy (531.0–533.6 eV) [40], denoted as O_{lat} and O_{sur}, respectively. The proportion of surface oxygen can be calculated by formula (2) [39]:

$$\frac{[\text{O}_{\text{sur}}]}{[\text{O}_{\text{sur}} + \text{O}_{\text{lat}}]} = \frac{\text{O}_{\text{sur}} \text{peak area}}{\text{Total peak area}} \quad (2)$$

The proportions of Ce³⁺, Ce⁴⁺, surface oxygen and lattice oxygen calculated from the formulas (1) and (2) are shown in Table 1. It can be seen from Table 1 that CeO₂-5 has the highest amount of surface oxygen as a result of its unique structure (composed of small size nano-CeO₂), large specific surface area and higher number of exposed atoms on the surface. Besides, the content of Ce³⁺ in this ceria is higher than the others, promoting the adsorption of benzyl alcohol on its surface. Compared with many literatures (see S6), CeO₂-5 has excellent comprehensive properties on the fraction of Ce³⁺ and specific surface area.

3.2. Catalytic activity

The direct coupling reactions of alcohol and amine catalyzed by the five ceria were conducted respectively. First, the influences of stirring rate were explored and the results were shown in S7. The initial conversion increased continuously with rotary speed rising, while stirring rate reached to 800 rpm, there was no obvious change on conversion. The Weisz-Prater Criterion also verified internal diffusion had little effect on this reaction. The rotate speed of follow-up experiments was

Table 1

The proportion of surface oxygen, lattice oxygen, Ce³⁺ and Ce⁴⁺ of ceria with different morphologies.

	CeO ₂ -1	CeO ₂ -2	CeO ₂ -3	CeO ₂ -4	CeO ₂ -5
Ce ³⁺	15%	23%	16%	13%	24%
Ce ⁴⁺	85%	77%	84%	87%	76%
O _{sur}	35%	48%	41%	33%	58%
O _{lat}	65%	52%	59%	67%	42%

Table 2

The catalytic ability of ceria with different morphologies on the reaction of benzyl alcohol and aniline.

Catalyst	S^a [$m^2 g^{-1}$]	Conversion [%]	Yield [%]	V^b [mmol $h^{-1} g^{-1}$]	$V \times 10^3 c$ [mmol $h^{-1} m^{-2}$]
None	–	0	0	–	–
CeO_2-1^d	33	23	18	0.075	2.273
CeO_2-2^d	88	94	83	0.346	3.930
CeO_2-3^d	15	23	20	0.083	5.556
CeO_2-4^d	64	0.34	0.25	0.001	0.016
CeO_2-5^d	162	≥ 99	≥ 99	–	–
CeO_2-5^e	162	≥ 99	≥ 99	0.825	5.093
CeO_2-5^f	162	92	89	0.742	4.578
CeO_2-5^g	162	≥ 99 ^h	≥ 99 ^h	0.550	3.395

^a Specific surface area was measured by N_2 -adsorption desorption (S8 & S9).

^b Formation rate per catalyst amount.

^c Formation rate per surface area.

^d Conditions: benzyl alcohol 1.0 mmol, aniline 2.0 mmol, ceria 100 mg, 800 rpm, 333 K, 24 h, air.

^e Ceria 50 mg, 800 rpm, 333 K, 24 h.

^f Ceria 50 mg, 800 rpm, 303 K, 24 h.

^g Ceria 50 mg, 800 rpm, 303 K, 36 h.

^h Repeated data of CeO_2-5 (S11).

fixed on 800 rpm to make sure that all the reactions were conducted under chemical control with negligible mass transport limitations. The products of this reaction were separated by column chromatography on silica gel using petroleum ether and ethyl acetate as eluent. All the 1H NMR and ^{13}C NMR spectra of the obtained solid proved that the products were benzalaniline (see S10). Table 2 shows the conversion and yield of the obtained five kinds of ceria catalyzing the reaction of benzyl alcohol and aniline at different conditions. When no ceria was added, benzyl alcohol and aniline didn't react with each other as there was no product found in the react system.

From Table 2, the conclusion can be drawn that these five kinds of ceria vary greatly in the catalytic ability on this reaction. The catalytic ability decreases in the following order: $CeO_2-5 > CeO_2-2 > CeO_2-3 \approx CeO_2-1 > CeO_2-4$, consistent with the order of H_2 -TPR results. The yield using CeO_2-5 as catalyst is 100 times more than that of CeO_2-4 . When the temperature is reduced to 303 K, CeO_2-5 with the highest specific surface area, still maintains a very high catalytic activity. The yield of benzalaniline can reach 89% when reacting for 24 h, which is higher than the results of long reaction time (48 h) reported by Tamura et al. And when the reaction time is prolonged to 36 h, the conversion of benzyl alcohol and the yield of benzalaniline can reach more than 99%. To our knowledge, CeO_2-5 is the best catalyst until now towards this reaction (see S12).

3.3. Roles of surface properties of nanoceria

As above, from the H_2 -TPR, pyridine-TPD, in-situ FTIR of adsorption pyridine, XPS and N_2 -adsorption desorption analysis along with the catalytic performance towards the imine synthesis of these five kinds of ceria, we found that their catalytic ability are influenced by amounts of acidic sites (especially Brønsted acidic sites), specific surface area as well as proportions of surface oxygen and Ce^{3+} ions. High specific surface area, high proportions of surface oxygen and Ce^{3+} ions of the catalyst are responsible for good catalytic performance. Besides, large amounts of acidic sites are also beneficial to the catalytic ability; and when the amounts of acidic sites are similar, the catalyst with stronger Brønsted acidic sites shows better catalytic performance.

Lewis and Brønsted acidic sites of CeO_2 , attributed to the surface Ce cations and acid OH groups respectively, could interact with oxygen atom of benzyl alcohol and weaken the chemical bond of O–H in benzyl alcohol molecule, especially Brønsted acidic sites [41–43], which are able to accelerate the oxidation of benzyl alcohol to form

benzaldehyde. The more surface acidic sites, the more adsorptions of benzyl alcohol.

It is commonly accepted that high catalytic activity of CeO_2 is related to its high oxygen storage capacity (OSC) and surface oxygen vacancies defect (OVD) [41,44]. High proportions of surface Ce^{3+} ions in CeO_2-5 implies that the redox potential between Ce^{4+} and Ce^{3+} cations is lower than others [1], which endows CeO_2-5 with the highest OSC in all these five CeO_2 . Meanwhile, high Ce^{3+} fraction in the surface indicates more OVDs, because in stoichiometric CeO_2 , oxygen has an oxidation state of 2-, it might transfer two electrons to cerium in order to maintain the electrostatic while oxygen leaves the surface, and then OVD and Ce^{3+} cations form [45]. OVD could add the adsorptions of O_2 , H_2O and benzyl alcohols. On the other hand, Ce^{3+} cations are also able to adsorb O_2 to form $Ce^{4+}-O_2^-$, and it is well known that O_2^- (superperoxo) are highly reactive electrophilic radical and can give rise to the increase of total oxidations [46,47]. The catalytic performance of CeO_2-5 following H_2 -TPR was tested and the conversion of benzyl alcohol at first four hours was zero while the conversion could be reach more than 40% when CeO_2-5 was used directly, and the final conversion (24 h) was also very low (13%). CeO_2-5 collected after H_2 -TPR experiment lost the chemisorbed oxygen species and some of the lattice oxygen species, so at the initial time it could not oxidize benzyl alcohol to benzaldehyde. These experimental results showed the importance of adsorbed oxygen species. The schematic diagram of roles of surface properties of nanoceria is shown in Fig. 4.

Moreover, it has been reported that if there are more –OH and OVD on the surface of metal oxides, they will have excellent ability to activate oxygen adsorbed on the surface [48]. High Brønsted acidic sites indicate that there are more –OH on the surface of CeO_2-5 . High Brønsted acidic sites together with high OVDs provide CeO_2-5 with outstanding catalytic performance.

In addition, the high specific surface area of CeO_2-5 also contributes to its catalytic property, because high specific surface area could afford more acidic sites, OVDs, Ce^{3+} cations and adsorbed active oxygen sequences.

3.4. Catalytic mechanism

Exploration of the catalytic mechanism of CeO_2-5 was performed by tracking the yield of product with different reaction time (S13) catalyzed by 50 mg CeO_2-5 at 333 K. Almost no accumulation of intermediate – benzaldehyde was found throughout the reacting process. We also studied the reactive process with different dosages of aniline in the same reactive conditions (S14). The increase in the amount of aniline led to high yield and conversion and no significant augment was found when benzyl alcohol/aniline rate was less than 1:2. Besides, there was almost no benzaldehyde detected after 24 h, when no aniline was added to the reaction system. Furthermore, the effects of CeO_2 on the reaction of benzaldehyde and aniline were investigated (S15), showing that all kinds of CeO_2 have almost no influence on this reaction.

In order to further illuminate the reaction mechanism of this reaction, DRIFTS was used, the results are shown in Fig. 5. As soon as benzyl alcohol was introduced on CeO_2 , bands at 1456 cm^{-1} (δ_{O-H}) and

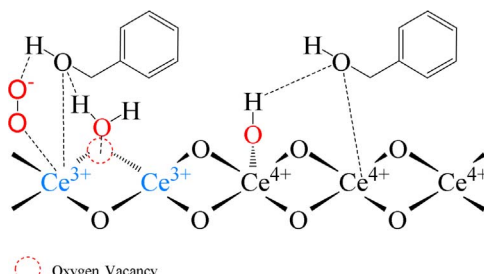


Fig. 4. Schematic diagram of roles of surface properties of nanoceria.

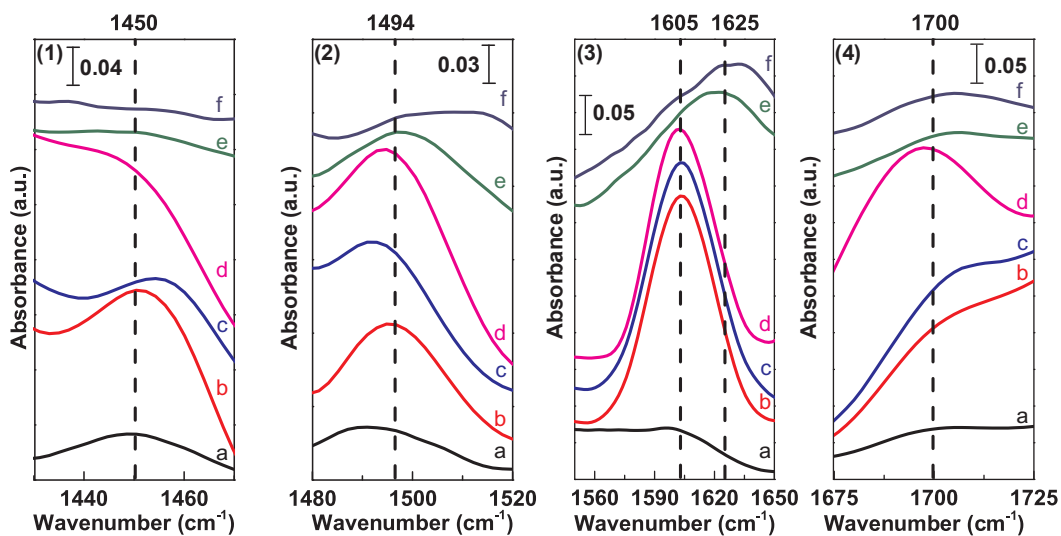


Fig. 5. Time-resolved FTIR spectra of CeO₂-5 in 1430–1470 cm⁻¹ (1), 1480–1520 cm⁻¹ (2), 1560–1650 cm⁻¹ (3) and 1675–1725 cm⁻¹ (4) region, respectively; at t = 0 s(a) 5 μL benzyl alcohol was injected into the in-situ IR cell to be adsorbed onto CeO₂, and the spectra were measured at 333 K under N₂ flow of 20 mL/min; once the spectra were stable (b), N₂ of 20 mL/min was replaced by air (c); 30 mins later (d), 10 μL aniline (e) was injected to the cell until the spectra was stable (f).

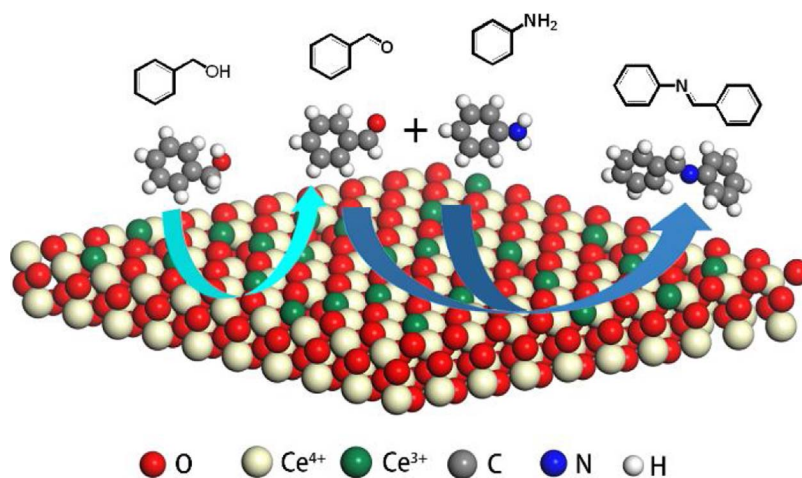


Fig. 6. Catalytic mechanism of benzyl alcohol and aniline catalyzed by ceria. (This is only a schematic diagram, not the real atomic arrangement).

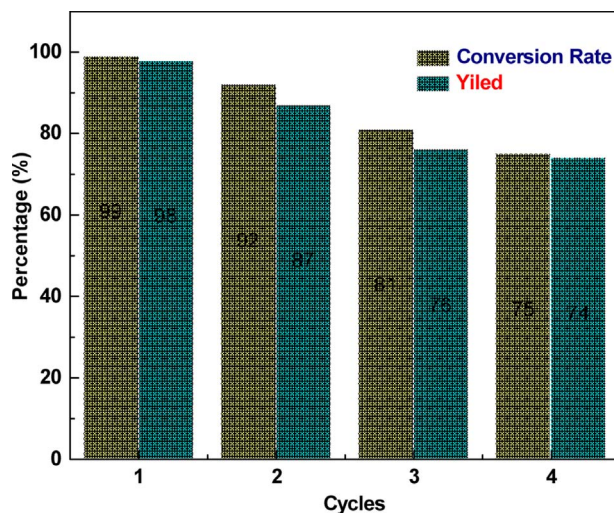


Fig. 7. Recycle test of CeO₂-5 for the synthesis of benzalaniline from benzyl alcohol and aniline. (Conditions: benzyl alcohol 1.0 mmol, aniline 2.0 mmol, Ceria 50 mg, 800 rpm, 333 K, air.).

1500 cm⁻¹ ($\nu_{C=C}$) were observed, which can be assignable to adspecies of benzyl alcohol on CeO₂. As time increased under N₂ flow, the bands intensities of 1456 cm⁻¹ began to decrease slowly, at the same time, the bands at 1605 cm⁻¹ and 1700 cm⁻¹ corresponding to $\nu_{C=C}$ and $\nu_{C=O}$ attached with carbonyl arose and their intensities increased gradually, indicating that benzyl alcohol could be directly oxidized by CeO₂ to benzaldehyde. At the end of N₂ introduction, the bands at 1456, 1500, 1605 and 1700 cm⁻¹ coexisted, CeO₂ was capable of oxidizing a part of benzyl alcohol into benzaldehyde. In addition, enhancement of the peak at 1700 cm⁻¹ and decrease of the band at 1456 cm⁻¹ were observed as the introduction of air, exhibiting that the oxidative dehydrogenation of benzyl alcohol to benzaldehyde was advanced by O₂ on CeO₂. However, the benzyl alcohol was not completely converted.

Furthermore, the injection of aniline (10 μL) resulted in new band at 1625 cm⁻¹ ($\nu_{C=N}$) and disappearance in 1605 cm⁻¹ as well as decrease in 1700 cm⁻¹ immediately, and the spectra went stable within 3 min without the appearance of band at 1456 cm⁻¹. The new band at 1625 cm⁻¹ ($\nu_{C=N}$) can be assigned to the adspecies of imines. This results indicated that the introduced aniline could react with benzaldehyde rapidly and with the decrease of benzaldehyde on the surface of CeO₂, the chemical equilibrium between benzyl alcohol and benzaldehyde was broken, the benzyl alcohol absorbed on CeO₂ could change to benzaldehyde and then react with aniline rapidly. The aniline could also serve as a promoter for the oxidation of benzyl alcohol to form

Table 3
Scope of alcohols and amines for the synthesis of imine.

Entry	Alcohol	Amine	Conversion [%] ^a	Yield [%] ^a	Conversion [%] ^b	Yield [%] ^b
1			33	32	98	95
2			18	17	> 99	97
3			29	29	> 99	98
4			32	27	99	93
5			17	14	80	78
6			33	26	> 99	95
7			27	24	96	94
8			22	17	96	84
9			28	26	> 99	94

^a Benzyl alcohol 10.0 mmol, aniline 20.0 mmol, CeO₂-5 0.5 g, 800 rpm, 333 K, 1 h, air.

^b Benzyl alcohol 10.0 mmol, aniline 20.0 mmol, CeO₂-5 0.5 g, 800 rpm, 333 K, 24 h, air.

benzaldehyde.

From the results of experiment and DRIFTS, we believe that the oxidation of benzyl alcohol on the surface of ceria is the rate-determining step in this reaction. At the same time, the reaction of benzyl alcohol catalytically oxidized to benzaldehyde is an equilibrium or reversible reaction, which can be accelerated by the addition of aniline. Similar enhancement caused by the addition of base was reported by the earlier research [49–51]. Besides, aniline can also work as reactant to imine formation, promoting the reaction by consuming benzaldehyde. The mechanism scheme of this reaction is shown in Fig. 6.

3.5. Magnification, recycling and universality of CeO₂-5

From both environmental and practical point of view, we studied the amplification of this reaction as the preparation process of CeO₂-5 is simple and feasible of scaling-up. The results show that the yield and conversion of the experiment of 10-fold magnification without any addition of solvent are both more than 99%, proving that the synthesis of benzylidene aniline catalyzed by the catalyst synthesized in this paper has good and environmentally-benign industry application prospects. We also studied the recycling of the catalyst. From the point of energy saving and environmental protection, CeO₂-5 was directly used after three times washing by alcohol and subsequent drying at 80 °C. The results are shown in Fig. 7. It can be seen that the catalyst has good recyclability, 4 cycles after the conversion of benzyl alcohol can still be maintained at more than 70%.

The 10-fold solvent-free reactions of benzyl alcohol derivatives and aniline derivatives catalyzed by CeO₂-5 at 333 K for 24 h were carried out to analyze its universality, as is shown in Table 3, presenting that this catalyst has good universality and catalytic activity for a scope of

imine synthesis by alcohols and amines. Aniline derivatives bearing either an electron-donating or an electron-withdrawing group reacted with benzyl alcohol (entries 1–4) to afford the adducts in good conversions and yields. The initial conversion of *p*-anisidine reacting with benzyl alcohol (entry 2) was low, however, the conversion could reach 82% after 8 h and the final conversion was very high. The possible reason may be that the interaction between oxygen atom in *p*-anisidine and active sites on the surface of ceria perhaps reduced the initial adsorbed amount of benzyl alcohols. Moreover, benzyl alcohol derivatives bearing both electron-donating and electron-withdrawing group reacted with aniline (entries 5–8) to produce the corresponding adducts in good conversions and yields. Besides, 2-naphthalenemethanol could also react with aniline in high conversion and yield (entry 9). From Table 3, it could also be found that no matter what substituted benzyl alcohols or aniline derivatives were there were a uniform law that electron-donating derivatives had good conversion and yield than electron-withdrawing groups. The oxygen atom in benzyl alcohol bearing electron-donating group had more electronegativity and could enhance the interaction between catalyst and alcohols, and then accelerate the oxidation of alcohols to aldehyde. While the nitrogen atom in aniline derivatives with electron-donating group had more electronegativity and this can accelerate the attacking abilities of nitrogen atom to carbon in carbonyl.

4. Conclusion

In this paper, five different ceria were synthesized by different methods, and the influencing rules of the ceria on the benzalaniline synthesis from benzyl alcohol and aniline were studied, indicating that higher specific surface area of ceria, stronger Brønsted acidic sites and

higher proportion of surface oxygen are responsible for the strong catalytic ability of ceria. CeO_2 -5 with large specific surface area and high surface oxygen content has the best catalytic activity, whose yield reaches more than 99% at 303 K for 36 h or at 333 K for 24 h, higher than the reported catalysts. From the results of experiment and DRIFTS, we know that the oxidation of benzyl alcohol on the surface of ceria is the rate-determining step in this reaction, and it can be accelerated by the addition of aniline by the consumption of benzaldehyde. Furthermore, CeO_2 -5 still shows excellent catalytic performance on the 10-fold magnification experiment without the addition of solvent. Besides, CeO_2 -5 has the advantages of simple process, low energy consumption and practical scaling-up as well as good universality towards this kind of reaction, showing every prospect in industrial application.

Acknowledgements

The authors are grateful for the financial support provided by the Science and Technology Project of Shenzhen (No. JCYJ20170306154725569), Science Foundation of Aeronautics of China (No. 2016ZF53059) and the Fundamental Research Funds for the Central Universities.

Appendix A. Supplementary data

Supplementary data associated with this article can be found, in the online version, at <https://doi.org/10.1016/j.apcata.2018.01.012>.

This material shows O_2 -TPD spectrum of CeO_2 -5, Pyridine-TPD spectra, Broad XPS spectra, Ce 3d XPS spectra, O 1s XPS spectra and N_2 adsorption and desorption isotherm of the five CeO_2 , the comparison of the fraction of Ce^{3+} and specific surface area, the effect of stirring rates on imine formation, NMR spectra of the obtained benzalaniline, the repeated XPS and SA analytic raw datum of CeO_2 -5, the repeated catalytic raw datum of CeO_2 -5 on benzalaniline formation, the comparison of conversion and on the reaction, other reaction profiles for benzalaniline, HPLC spectrum of the obtained mixture.

References

- A. Trovarelli, Catalytic properties of ceria and CeO_2 -containing materials, *Catal. Rev.* 38 (1996) 439–520.
- J. Paier, C. Penschke, J. Sauer, Oxygen defects and surface chemistry of ceria: quantum chemical studies compared to experiment, *Chem. Rev.* 113 (2013) 3949–3985.
- H. Zhang, W. Wang, B. Zhang, H. Li, Q. Zhang, Controllable synthesis of spherical cerium oxide particles, *RSC Adv.* 6 (2016) 30956–30962.
- Z. Zhang, Y. Wang, J. Lu, C. Zhang, M. Wang, M. Li, X. Liu, F. Wang, Conversion of isobutene and formaldehyde to diol using praseodymium-doped CeO_2 catalyst, *ACS Catal.* 6 (2016) 8248–8254.
- A. Corma, P. Atienzar, H. Garcia, Hierarchically mesostructured doped CeO_2 with potential for solar-cell use, *Nat. Mater.* 3 (2004) 394–397.
- H. Zhang, B. Yang, H. Li, C. Wu, W. Wang, B. Zhang, Q. Zhang, C. Zhang, *Cryst. Res. Technol.* (2017) 1700233, <http://dx.doi.org/10.1002/crat.201700233>.
- A.A.A. da Silva, N. Bion, F. Epron, Effect of the type of ceria dopant on the performance of Ni/ CeO_2 SOFC anode for ethanol internal reforming, *Appl. Catal. B: Environ.* 206 (2017) 626–641.
- S.D. Park, J.M. Vohs, R.J. Gorte, Direct oxidation of hydrocarbons in a solid-oxide fuel cell, *Nature* 404 (2000) 265–267.
- L. Adjianto, A. Sampath, A.S. Yu, M. Cargnello, P. Fornasiero, R.J. Gorte, J.M. Vohs, Synthesis and stability of $\text{Pd}@\text{CeO}_2$ core-shell catalyst films in solid oxide fuel cell anodes, *ACS Catal.* 3 (2013) 1801–1809.
- A. Uzunoglu, H. Zhang, S. Andreescu, L.A. Stanciu, CeO_2 – MO_x (M: Zr, Ti, Cu) mixed metal oxides with enhanced oxygen storage capacity, *J. Mater. Sci.* 50 (2015) 3750–3762.
- I. Heo, M.H. Wiebenga, J.R. Gaudet, I.S. Nam, W. Li, C.H. Kim, Ultra low temperature CO and HC oxidation over Cu-based mixed oxides for future automotive applications, *Appl. Catal. B: Environ.* 160 (2014) 365–373.
- P. Hartmann, T. Brezesinski, J. Sann, A. Lotnyk, J. Eufinger, L. Kienle, J. Janek, Defect chemistry of oxide nanomaterials with high surface area: ordered mesoporous thin films of the oxygen storage catalyst CeO_2 – ZrO_2 , *ACS Nano* 7 (2013) 2999–3013.
- Y. Zhou, L. Lan, M. Gong, Y. Chen, Modification of the thermal stability of doped CeO_2 – ZrO_2 mixed oxides with the addition of triethylamine and its application as a Pd-only three-way catalyst, *J. Mater. Sci.* 51 (2016) 4283–4295.
- F. Wang, X. Wang, D. Liu, J. Zhen, J. Li, Y. Wang, H. Zhang, High-performance $\text{ZnCo}_2\text{O}_4@\text{CeO}_2$ core@shell microspheres for catalytic CO oxidation, *ACS Appl. Mater. Interfaces* 6 (2014) 22216–22223.
- Y. Lin, Z. Wu, J. Wen, K.R. Poeppelmeier, L.D. Marks, Imaging the atomic surface structures of CeO_2 nanoparticles, *Nano Lett.* 14 (2013) 191–196.
- R.J. Gorte, Ceria in catalysis: from automotive applications to the water–gas shift reaction, *AIChE J.* 56 (2010) 1126–1135.
- U. Tumuluri, G. Rother, Z. Wu, Fundamental understanding of the interaction of acid gases with CeO_2 : from surface science to practical catalysis, *Ind. Eng. Chem. Res.* 55 (2016) 3909–3919.
- Y. Liu, B. Liu, Improvement of catalytic performance of preferential oxidation of CO in H_2 -rich gases on three-dimensionally ordered macro-and meso-porous Pt-Au/ CeO_2 catalysts, *Appl. Catal. B: Environ.* 142 (2013) 615–625.
- I. Cabeza, L.G. Souto, J.M. Pintado, C. Pereira, C. Freire, G. Blanco, Influence of ceria distribution on the redox behaviour of nanoparticulated CeO_2 – SiO_2 systems with application in catalysis, *Surf. Interface Anal.* 46 (2014) 712–715.
- Y. Liu, H. Chen, J. Li, P. Yang, Morphology adjustment of one dimensional CeO_2 nanostructures via calcination and their composite with Au nanoparticles towards enhanced catalysis, *RSC Adv.* 5 (2015) 37585–37591.
- G. Vile, S. Colussi, F. Krumeich, A. Trovarelli, J. Perez-Ramirez, Opposite face sensitivity of CeO_2 in hydrogenation and oxidation catalysis, *Angew. Chem. Int. Ed.* 53 (2014) 12069–12072.
- D. Gamarra, A.L. Cámara, M. Monte, Preferential oxidation of CO in excess H_2 over CuO/CeO_2 catalysts: characterization and performance as a function of exposed face present in the CeO_2 support, *Appl. Catal. B: Environ.* 130 (2013) 224–228.
- K. Mudiyanselage, I. Al-Shankiti, A. Fouli, J. Llorca, H. Idriss, Reactions of ethanol over CeO_2 and Ru/ CeO_2 catalysts, *Appl. Catal. B: Environ.* 197 (2016) 198–205.
- A. Corma, M.E. Domíne, Gold supported on a mesoporous CeO_2 matrix as an efficient catalyst in the selective aerobic oxidation of aldehydes in the liquid phase, *Chem. Commun.* 32 (2005) 4042–4044.
- M.J. Beier, T.W. Hansen, J. Grunwaldt, Selective liquid-phase oxidation of alcohols catalyzed by a silver-based catalyst promoted by the presence of ceria, *J. Catal.* 266 (2009) 320–330.
- T. Wang, X. Yuan, S. Li, L. Zeng, J. Gong, CeO_2 -modified Au@SBA-15 nanocatalysts for liquid-phase selective oxidation of benzyl alcohol, *Nanoscale* 7 (2015) 7593–7602.
- S.I. Murahashi, Synthetic aspects of metal-catalyzed oxidations of amines and related reactions, *Angew. Chem. Int. Ed.* 34 (1995) 2443–2465.
- S. Yao, S. Saaby, R.G. Hazell, K.A. Jørgensen, Catalytic enantioselectiveaza-diels-alder reactions of imines—an approach to optically active nonproteinogenic α -amino acids, *Chem. A Eur. J.* 6 (2000) 2435–2448.
- Z. Liu, Y. Wang, Z. Li, J. Jiang, D.W. Boykin, Synthesis and anticancer activity of novel 3, 4-diarylhiazol-2(3H)-ones (imines), *Bioorg. Med. Chem. Lett.* 19 (2009) 5661–5664.
- B. Chen, L. Wang, S. Gao, Recent advances in aerobic oxidation of alcohols and amines to imines, *ACS Catal.* 5 (2015) 5851–5876.
- R. He, X. Jin, H. Chen, Z. Huang, Q. Zheng, C. Wang, Mn-catalyzed three-component reactions of imines/nitriles, grignard reagents, and tetrahydrofuran: an expedient access to 1,5-amino/keto alcohols, *J. Am. Chem. Soc.* 136 (2014) 6558–6561.
- M. Tamura, K. Tomishige, Redox properties of CeO_2 at low temperature: the direct synthesis of imines from alcohol and amine, *Angew. Chem. Int. Ed.* 54 (2015) 864–867.
- C. Pan, D. Zhang, L. Shi, J. Fang, Template-free synthesis, controlled conversion, and CO oxidation properties of CeO_2 nanorods nanotubes, nanowires, and nanocubes, *Eur. J. Inorg. Chem.* 2008 (2008) 2429–2436.
- F. Liu, H. He, Structure-activity relationship of iron titanate catalysts in the selective catalytic reduction of NO_x with NH_3 , *J. Phys. Chem. C* 114 (2010) 16929–16936.
- O.M. Busch, W. Brijoux, S. Thomson, F. Schüth, Spatially resolving infrared spectroscopy for parallelized characterization of acid sites of catalysts via pyridine sorption: possibilities and limitations, *J. Catal.* 222 (2004) 174–179.
- B.H. Davis, R.A. Keogh, S. Alerasoool, D.J. Zalewski, D.E. Day, P.K. Doolin, Infrared study of pyridine adsorbed on unpromoted and promoted sulfated zirconia, *J. Catal.* 183 (1999) 45–52.
- D.R. Mullins, S.H. Overbury, D.R. Huntley, Electron spectroscopy of single crystal and polycrystalline cerium oxide surfaces, *Surf. Sci.* 409 (1998) 307–319.
- H. Borchert, Y.V. Frolova, V.V. Kaichev, I.P. Prosvirin, G.M. Alikina, A.I. Lukashevich, V.I. Zaikovskii, E.M. Moroz, S.N. Trukhan, V.P. Ivanov, E.A. Paukshtis, V.I. Bukhtiyarov, V.A. Sadykov, Electronic and chemical properties of nanostructured cerium dioxide doped with praseodymium, *J. Phys. Chem. B* 109 (2005) 5728–5738.
- B. Xu, Q. Zhang, S. Yuan, M. Zhang, T. Ohno, Morphology control and characterization of broom-like porous CeO_2 , *Chem. Eng. J.* 260 (2015) 126–132.
- H. Borchert, Y. Borchert, V.V. Kaichev, I.P. Prosvirin, G.M. Alikina, A.I. Lukashevich, V.I. Zaikovskii, E.M. Moroz, E.A. Paukshtis, V.I. Bukhtiyarov, V.A. Sadykov, Nanostructured, Gd-doped ceria promoted by Pt or Pd: investigation of the electronic and surface structures and relations to chemical properties, *J. Phys. Chem. B* 109 (2005) 20077–20086.
- Z. Wu, A.K.P. Mann, M. Li, Spectroscopic investigation of surface-dependent acid-base property of ceria nanoshapes, *J. Phys. Chem. C* 119 (2015) 7340–7350.
- J.A. Lercher, C. Gründling, G. Eder-Mirth, Infrared studies of the surface acidity of oxides and zeolites using adsorbed probe molecules, *Catal. Today* 27 (1996) 353–376.
- S. Higashimoto, K. Okada, T. Morisugi, Effect of surface treatment on the selective photocatalytic oxidation of benzyl alcohol into benzaldehyde by O_2 on TiO_2 under visible light, *Top. Catal.* 53 (2010) 578–583.

[44] N.J. Lawrence, J.R. Brewer, L. Wang, Defect engineering in cubic cerium oxide nanostructures for catalytic oxidation, *Nano Lett.* 11 (2011) 2666–2671.

[45] S. Deshpande, S. Patil, S.V.N.T. Kuchibhatla, Size dependency variation in lattice parameter and valency states in nanocrystalline cerium oxide, *Appl. Phys. Lett.* 87 (2005) 133113.

[46] D.R. Mullins, The surface chemistry of cerium oxide, *Surf. Sci. Rep.* 70 (2015) 42–85.

[47] H. Pan, Y. Jian, C. Chen, Sphere-shaped Mn_3O_4 catalyst with remarkable low-temperature activity for methyl-ethyl-ketone combustion, *Environ. Sci. Technol.* 51 (2017) 6288–6297.

[48] F. Cheng, T. Zhang, Y. Zhang, Enhancing electrocatalytic oxygen reduction on MnO_2 with vacancies, *Angew. Chem. Int. Ed.* 52 (2013) 2474–2477.

[49] M.M. Kadam, K.B. Dhopate, N. Jha, V.G. Gaikar, P.R. Nemade, Synthesis, characterization and application of γ - MnO_2 /graphene oxide for the selective aerobic oxidation of benzyl alcohols to corresponding carbonyl compounds, *New J. Chem.* 40 (2016) 1436–1442.

[50] S. Rautiainen, O. Simakova, H. Guo, A. Leino, K. Kordás, D. Murzin, M. Leskelä, T. Repo, Solvent controlled catalysis: synthesis of aldehyde, acid or ester by selective oxidation of benzyl alcohol with gold nanoparticles on alumina, *Appl. Catal. A: Gen.* 485 (2014) 202–206.

[51] J. Zhu, P.C. Wang, M. Lu, Selective oxidation of benzyl alcohol under solvent-free condition with gold nanoparticles encapsulated in metal-organic framework, *Appl. Catal. A: Gen.* 477 (2014) 125–131.